ELSEVIER

International Journal of Heat and Fluid Flow 20 (1999) 437–445

International Journal of HEAT AND FLUID FLOW

www.elsevier.com/locate/ijhff

2-D kettle reboiler circulation model

B.M. Burnside *

Department of Mechanical and Chemical Engineering, Heriot-Watt University, Riccarton, Edinburgh EH14 4AS, UK

Received 20 June 1998; accepted 11 February 1999

Abstract

A 2-D model is developed for sections of a kettle reboiler where liquid/vapour disengagement is not severe. Using a trial set of boundary conditions it is shown that the influence of flow around the periphery of the bundle has negligible effect on flow distribution over the tubes. Uniform heat flux solutions are obtained for $q = 20$ and 50 kW/m^2 boiling pentane and R113 at 1 atm. Pronounced 2-D effects were obtained at the higher heat flux only. Use of typical superposition and asymptotic flow boiling correlations resulted in bundle average heat transfer coefficients for both heat fluxes no different from the values predicted by the 1-D model. However, it is suggested that the 2-D solution mass velocity and void fraction distribution are important for predicting the design maximum heat flux limitation.

Keywords: Kettle reboilers; Heat transfer; 2-D design

Notation

AR	area ratio
C	velocity, m/s
C_d	interfacial friction coeff.
D	tube o.d., m
F	body force, N/m^3, flow factor
Fr	Froude no.
g	gravitational acceleration, m/s^2
G	mass velocity, kg/s m^2
GY, GZ	mass velocities in y, z directions, kg/s m^2
GB, GT	mass velocity at bottom and top of bundle, kg/s m^2
h	enthalpy, kJ/kg
H	bundle height, m
i, j	cell identification numbers
k	thermal conductivity, kW/m K
m, n	Reynolds no. index in single phase convection and friction factor correlation
MF	momentum flux/unit area, N/m^2
N_C	number of tube columns
N_R	number of tube rows
P	pressure, N/m^2
q	heat flux density, kW/m^2
S	suppression factor
s	pitch, m
v, w	velocities in y and z directions, m/s
W	bundle width, m
x	quality
X_0	constant, Eq. (16), m
y, z	horizontal and vertical directions

Greek

α	heat transfer coefficient, kW/m^2 K
ϵ	void fraction
Φ	rate of heat interaction/unit volume, kW/m^2/m
ϕ_l^2	2-phase friction multiplier
μ	viscosity, kg/m s
ρ	density, kg/m^3
σ	standard deviation

Subscripts

av	average
b, bot	bottom of bundle
c	single phase convection
fb	flow boiling
fric	friction
flo	liquid, flowing alone
g	gravitational
H	homogeneous 2-phase flow
h	horizontal
l	liquid
m	momentum
md	momentum drag
max	maximum value based on minimum flow area
npb	nucleate pool boiling
t	top
v	vertical, vapour
y, z	coordinate direction

1. Introduction

In the design of kettle reboilers and chiller evaporators process intensification dictates reduced ΔT between heating and heated fluids. A consequence is that thermo-hydraulic

* Tel.: +44 131 449 5111; fax: +44 131 451 3129

0142-727X/99/$ – see front matter
PII: S0142-727X(99)00024-7

design on the shell side has become more critical. Although flow in kettle reboilers is strictly 3-dimensional (3-D), as illustrated by Brisbane et al. (1980) and Palen and Yang (1981), commercial design codes confine analysis to a number of sections along the bundle assuming that it moves only in a vertical plane and further, that it is 1-D. A simple 1-D circulation model calculation shows that the vertical pressure gradient within the bundle is not constant, causing a lateral pressure gradient, which must be satisfied by a lateral flow, as has been observed experimentally by Cornwell et al. (1980), Shire (1995) and King and Jensen (1995).

To date, a number of investigators have applied CFD codes to the kettle reboiler configuration. Carlucci et al. (1984) employed a method similar to that used by Carlucci and Sutherland (1981) and by Singhal and Spalding (1979) to predict the distribution of flow in nuclear reactor evaporators. The 2-phase flow is based either on the algebraic-slip model, where liquid and vapour are assumed to move in the same direction but can have unequal velocities, or 2-fluid models, where liquid and vapour phases may move in different directions. As in the 1-D recirculation models, the 2-phase flow can be considered to be homogeneous, as assumed by Carlucci et al. (1984) or separated as assumed by Carlucci and Sutherland (1981), Singhal and Spalding (1979) and Edwards and Jensen (1991). Observation of 2-phase cross-flow in reboiler bundles by Hadi and Burnside (1992), Schrage et al. (1988) and Dowlati et al. (1992a) establishes that there is slip between vapour and liquid. Separated flow models with appropriate void fraction correlations as developed by Schrage et al. (1988) are therefore necessary. Carlucci et al. (1984) modelled the experimental kettle reboiler thin slice used by Cornwell et al. (1980), boiling R113 at 1 atm with $q = 20$ kW/m^2. Their general technique set the porosity constant within the bundle and included an elaborate system to determine it on the bundle boundaries. Loss coefficient in the horizontal and vertical momentum equations within and without the bundle were dependent on the local porosity and friction factor defined in terms of the free stream dynamic head. A velocity field was predicted similar to that deduced from observations by Cornwell et al. (1980), but, since homogeneous 2-phase flow was assumed, the recirculation mass velocity was higher than measured both by this and a later optical method used by Shire et al. (1994).

Fundamental 2-fluid treatments, such as that of Lahey and Drew (1988) require simultaneous generation of the nature and geometry of the flow but this is impossible at present for the flow in reboiler bundles. The two-fluid model of Singhal and Spalding (1979) is an example of the limits to which this approach can be taken. Edwards and Jensen (1991) used this method, based on the PHOENICS CFD code, in an attempt to predict the results of Cornwell et al. (1980). Specification of the interfacial drag coefficient was critical to the results and, at the lowest value for which solutions could be obtained, void fraction was still 30% above the measurements. However, the pattern of flow at the side of the bundle agreed with values reported by the experiments.

More recently Rahman et al. (1996) refined this work by relating the interfacial drag coefficients, C_d, to pressure drop and void fraction for crossflow over tube bundles as measured by Schrage et al. (1988) and Dowlati et al. (1990, 1992b). For a given porosity, C_d was found to have a power law dependence on a Reynolds number $\mathrm{Re} = (\rho_m C_v \delta_l)/\mu_l$, where the characteristic length, $\delta_l = \text{porosity} \times s_h$. Although the scatter of the data was high, the authors maintained that when the correlation was employed in subsequent predictions, this had little effect. The Cornwell et al. (1980) (R113 at 1 atm, $q = 20$ kW/m^2) observation of an apparently very rapid increase in void fraction over lines starting about one-third of the way up the bundle at the centre to the edges of the bundle a few rows from the top was predicted by this method.

King and Jensen (1995) have drawn attention to the effect of foam formation in and around the top rows of experimental bundles due to the difficulties of disengagement in this slice experimental configurations. In their experiments the reboiler slice was 159 mm long, with a 75 tube half bundle uniformly heated with $q = 10$–70 kW/m^2. At heat fluxes as low as 10 kW/m^2 bubbles circulated more than halfway down the space between bundle and shell with a high voidage region above. The disengagement problem built up with rise in heat flux. At 30 kW/m^2, only a very small region near the bottom of the shell was free of vapour and there was a frothy vertical downflow into the centre of the top row of the bundle.

Does this pattern of flow occur in full size kettle reboilers? The weir and much increased shell cross sectional area at the vapour outlet end are different substantially from the experimental configurations. King and Jensen's rig had a cylindrical shell, 171 mm long, of a single diameter with a small outlet at the top (King and Jensen, 1995). Although the estimated vapour exist velocity is low, the restricted space above the bundle caused the flow of fluid to be directed towards the centre of the shell and downwards into the bundle producing the observed trapped thick layer of "froth". This author feels that over most of the shell length this behaviour is unlikely to occur in commercial kettle reboilers, particularly at high pressures.

This paper is aimed at full scale kettle reboiler performance prediction. In line with the above discussion, it is assumed that:

1. There is no substantial build-up of foam at the sides of the bundle below the top row of tubes. Consequently, any ingress of fluid into the top rows is liquid only.
2. An algebraic slip separated flow model can represent the 2-phase flow around the tubes of the bundle.

The object of this paper is to determine shellside 2-D crossflow effects in the bundle. Further, the extent of the influence of conditions outside the bundle on the flow within it needs to be evaluated before determining the sophistication necessary in computation for design. This is investigated below by determining the response of flow in the bundle to the pressure and velocity fields on its boundary.

2. 2-D recirculation model

The bundle is assumed to be rectangular and situated in a pool of saturated liquid. Analysis is confined to one half of the shellside space about the vertical centre line. Boundary conditions which must be specified are:

1. distribution of pressure at the side and bottom of the bundle;
2. distribution of vertical component of velocity at the side of the bundle;
3. distribution of horizontal component of velocity above and below the bundle;
4. zero horizontal component of velocity on the vertical centre line.

The vapour/liquid interface level is assumed to be one half vertical tube pitch above the centre of the top row of tubes and the pool at the side of the bundle to be liquid only. This is equivalent to ignoring the effect of phase disengagement on the difference between the pressure head of fluid above the bundle and that in the pool at the side of the bundle. Conditions (1)–(3) recognise that shellside flow within the bundle must induce movement in the adjacent fluid. In practice, this will be affected by the presence of shell walls. It is recognised that the rectangular bundle shape is not a good representation of small bundles but in full scale reboilers there is a smaller proportion of tubes in short columns.

Uniform heat flux conditions are postulated to de-couple the flow field solution from the flow boiling correlations. No dry-out correlation is included in the solution. An in-line bundle configuration is modelled, Fig. 1, with rectangular cells surrounding each tube, Fig. 2, boundaries equidistant between tubes. The solution obtained here is for a square pitch configuration with 19 mm diameter tubes and 1.33 pitch:diameter ratio. The half bundle has 17 rows and 9 columns. This is the configuration used by Cornwell et al. (1980) and Shire et al. (1994).

An algebraic slip model is assumed. The conservation conditions are as follows.

Continuity:

$$\frac{\partial(\rho w)}{\partial z}+\frac{\partial(\rho v)}{\partial y}=0.$$

Momentum:

$$\frac{\partial(\rho w^2)}{\partial z}+\frac{\partial(\rho wv)}{\partial y}=-\frac{\partial P}{\partial z}-\rho g-F_z$$

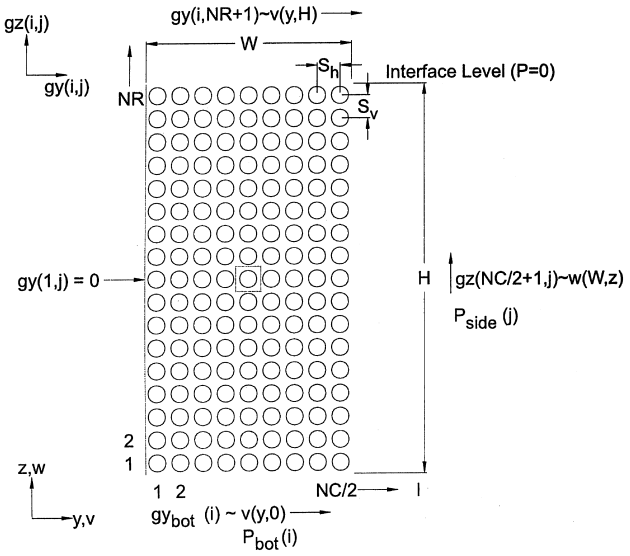

Fig. 1. 2-D reboiler model.

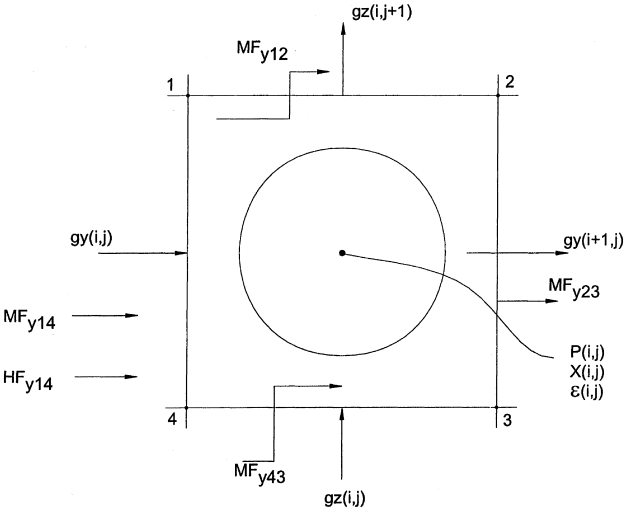

Fig. 2. Cells used in 2-D reboiler model.

$$\frac{\partial(\rho vw)}{\partial z}+\frac{\partial(\rho v^2)}{\partial y}=-\frac{\partial P}{\partial y}-F_y.$$

Energy:

$$\frac{\partial(\rho wh)}{\partial z}+\frac{\partial(\rho vh)}{\partial y}=\Phi,$$

where Φ is uniform equal to $\pi Dq/s_{\mathrm{h}}s_{\mathrm{v}}$. Shear force terms have been neglected in the momentum equations. The largest velocities predicted are about 0.3 m/s and the cell dimensions are 25.4 mm. In the worst case, therefore, the double gradients of velocity cannot exceed ≈ 2000 m/s m^2. The viscosity of liquid pentane is of the order 10^{-4} kg/m s. Thus the maximum pressure gradient required to balance the shear forces is less than 0.2 Pa/m, negligible.

Boundary conditions (Fig. 1):

$$\begin{array}{ll} y=0: & v(0,z)=0 \text{ (symmetry)},\\ y=W: & w=w(W,z), P=P(W,z), h(W,z)=h_{\mathrm{l}},\\ z=0: & v=v(y,0), P=P(y,0), h(y,0)=h_{\mathrm{l}},\\ z=H: & v=v(y,H), P=0. \end{array}$$

The conservation equations are discretised on the basis of rectangular cross section control volumes, side $s_{\mathrm{h}}, s_{\mathrm{v}}$, and unit length, surrounding each tube, Fig. 2. Velocities are defined in the middle of cell boundaries and pressure, quality and void fraction at the centre of the cell. The integrated equations are shown below for cell (i,j) of a square pitched configuration, $s=s_{\mathrm{h}}=s_{\mathrm{v}}$.

Continuity:

$$\mathrm{GZ}(i,j)+\mathrm{GY}(i,j)-\mathrm{GZ}(i,j+1)-\mathrm{GY}(i+1,j)=0. \tag{1}$$

Momentum: In the y direction

$$\{(\mathrm{MF}_{y23})-(\mathrm{MF}_{y41})\}+\{(\mathrm{MF}_{y12})-(\mathrm{MF}_{y43})\} =-\Delta P_y-\Delta P_{\mathrm{fric}y}, \tag{2}$$

where ΔP_{fric} is the friction pressure *drop* due to the presence of tubes in the cell. Brisbane et al. (1980) called the first term on the L.S. of Eq. (2) a momentum pressure drop, ΔP_{my} and the second term may be called a momentum drag pressure drop ΔP_{mdy}. Hence, the pressure drops through the cell (i,j) in the y and z directions are

$$-\Delta P_y=\Delta P_{\mathrm{my}}+\Delta P_{\mathrm{mdy}}+\Delta P_{\mathrm{fric}y}, \tag{3}$$

$$-\Delta P_z=\Delta P_{\mathrm{g}}+\Delta P_{\mathrm{mz}}+\Delta P_{\mathrm{mdz}}+\Delta P_{\mathrm{fric}z}, \tag{4}$$

where ΔP_{g} is the gravitational pressure drop with height through the cell.

Energy:

$$\{\mathrm{GY}(i+1,j)x_{23}-\mathrm{GY}(i,j)x_{14}\} +\{\mathrm{GZ}(i,j+1)x_{12}-\mathrm{GZ}(i,j)x_{43}\}=\frac{\pi qD}{sh_{\mathrm{lv}}}, \tag{5}$$

where quality at the top boundary of cell (i,j), for example, is the arithmetic mean of the value in the cell and in the one above.

The boundary conditions are:

- $\mathrm{GZ}(N_{\mathrm{C}}/2+1,j)$, $(j=1,N_{\mathrm{R}})$, $\mathrm{GY}_{\mathrm{bot}}(i)$ and $\mathrm{GY}(i,N_{\mathrm{R}}+1)$, $(i=1,N_{\mathrm{C}}/2)$ defined.
- $P_{\mathrm{side}}(j)$, $(j=1,N_{\mathrm{R}})$ and $P_{\mathrm{bot}}(i)$, $(i=1,N_{\mathrm{C}}/2)$, both given.

The qualities x_{lm} to be used at the boundaries, Fig. 1, depend on the direction of flow. At the bottom $x_{43}=0$ since $\mathrm{GZ}(1,j)>0$. At the top $x_{12}=x(i,N_{\mathrm{R}})$ and at the side $x_{32}=0$ if $\mathrm{GY}(N_{\mathrm{C}}/2+1,j)<0$ or $x(N_{\mathrm{C}}/2,j)$ otherwise.

3. Solution procedure

Using an initial guess of $GZ(i,1)$ $(i = 1, N_C/2)$ at entry to the first row, all the horizontal components, $GY(i,j)$ were set to zero.

In all the solutions attempted here, pressures $P_{side}(j)$ and $P_{bot}(i)$ were set to the hydrostatic pressures $P_B\{1-(j-0.5)/N_R\}$ and P_B, respectively, where $P_B = \rho_l g N_R s_v$. This choice is investigated later. Various boundary conditions $GY_{bot}(i)$, $GY(i, N_R+1)$ and $GZ(N_C/2+1, j)$ were imposed. For the fixed current $GY(i,j)$ distribution, using Newton's method, the range of mass velocities $GZ(i,j)$, in each column was determined, such that the total pressure drops due to gravitational, momentum and friction balanced the hydrostatic head in the pool outside the bundle, Eq. (4). The pressures in each cell were calculated in two ways:

1. P_{bot} and the *vertical* total of the pressure *rises*, $\Delta P_z(i,j)$, in the z-direction

$$P_z(i,j) = P_{bot} + 0.5\Delta P_z(i,1) + \sum_{j=2}^{j} 0.5\{\Delta P_z(i,j-1) + \Delta P_z(i,j)\}.$$

2. P_{side} and the *horizontal* total pressure rises, $\Delta P_y(i)$, in the y-direction

$$P_y(i,j) = P_{side}(j) - 0.5\Delta P_y(N_C/2, j) - \sum_{i=\frac{N_C}{2}-1}^{i} 0.5\{\Delta P_y(i,j) + \Delta P_y(i+1,j)\}.$$

The objective is to match these two pressure fields by varying $GY(i,j)$. First the standard deviation of the fractional pressure differences, $\sigma\{1 - P_y(i,j)/P_z(i,j)\}$, was calculated. A Newton–Broyden iteration then scanned the cells, calculating new values of $GY(i,j)$. This continued until σ was reduced to below 10^{-9}. The complete solution took only a few seconds of computer time.

3.1. Pressure drops

Qualities, $x(i,j)$ were calculated using Eq. (5). Starting with an initial guess, the cells were scanned row-by-row. The process was repeated until the largest fractional difference between successive values was small enough. At a later stage this method was replaced by a matrix solution of the $N_R N_C/2$ energy equations (5), making use of the band diagonal character of the matrix of coefficients of the qualities. The Schrage et al. (1988) correlation was used to calculate the void fractions,

$$\epsilon = \epsilon_H\left\{1 + 0.123\frac{\ln x}{Fr^{0.191}}\right\}, \tag{6}$$

where ϵ_H is the homogeneous flow value and $Fr = G/\rho_l(gD)^{0.5}$. Eq. (6) was devised for use with air/water and R113 systems. Unpublished vertical crossflow pressure drop data measured in this author's laboratory showed that it was equally successful used for pentane in conjunction with the Ishihara et al. (1980) 2-phase friction multiplier correlation referred to below. In applying Eq. (6) the vector value of G was used, although the experiments on which it is based were for vertical crossflow. This is justified on the basis that the flow is predominantly vertical. Pressure drop terms were evaluated as follows.

3.1.1. Gravitational pressure drop

$\Delta P_g = g s_v \rho_{tp}$,

where

$\rho_{tp} = \rho_v\epsilon + \rho_l(1-\epsilon)$.

3.1.2. Momentum pressure drops

$$\Delta P_{mz}(i,j) = \{GZ(i,j+1)\}^2\left\{\frac{x_{12}^2}{\rho_v\epsilon_{12}} + \frac{(1-x_{12})^2}{\rho_l(1-\epsilon_{12})}\right\} - \{GZ(i,j)\}^2\left\{\frac{x_{43}^2}{\rho_v\epsilon_{43}} + \frac{(1-x_{43})^2}{\rho_l(1-\epsilon_{43})}\right\}.$$

In the same way an equation can be written for $\Delta P_{my}(i,j)$. In this case $GY(i+1,j)$ and $GY(i,j)$ may both be −ve or of opposite sign.

3.1.3. Momentum drag pressure drops

In this case mass velocities along the cell boundaries at their centres, GZ_{41}, GZ_{32}, GY_{12}, GY_{43} are required. These are taken to be the arithmetic average of the four adjacent defined values. For a cell (i,j) in the bundle interior

$\Delta P_{mdz}(i,j) = (MF_{lz32} - MF_{lz41})$,

where, for the liquid phase

$$MF_{lz41} = GY(i,j)(1-x_{41})^2\frac{GZ_{41}}{\rho_l(1-\epsilon_{41})}, \tag{7}$$

$$MF_{lz32} = GY(i+1,j)(1-x_{32})^2\frac{GZ_{32}}{\rho_l(1-\epsilon_{32})} \tag{8}$$

with similar expressions for the vapour phase. Also

$\Delta P_{mdy}(i,j) = (MF_{ly12} - MF_{ly43})$,

where, for the liquid phase,

$$MF_{ly43} = GZ(i,j)(1-x_{43})^2\frac{GY_{43}}{\rho_l(1-\epsilon_{43})}, \tag{9}$$

$$MF_{ly12} = GZ(i,j+1)(1-x_{12})^2\frac{GY_{12}}{\rho_l(1-\epsilon_{12})} \tag{10}$$

again with similar expressions for the vapour phase. x_{lm} and ϵ_{lm} are the values at the centres of the cell walls lm. At top, bottom and sides of the bundle the appropriate qualities (see Section 2) must be used in Eqs. (7)–(10).

3.1.4. Friction pressure drops

Friction pressure drops were calculated using the vector velocity and the approximation that liquid only pressure drops and the 2-phase friction multiplier were the same as if the flow were purely vertical. Thus the liquid alone pressure drop, ΔP_{flo}, was calculated using ESDU 79034 (ESDU, 1979) and the 2-phase multiplier, ϕ_l^2, using the correlation of Ishihara et al. (1980),

$$\phi_l^2 = 1 + \frac{8}{X_{tt}} + \frac{1}{X_{tt}^2}, \tag{11}$$

where X_{tt} is the Martinelli parameter

$$X_{tt} = \left\{\frac{1-x}{x}\right\}^{0.9}\left\{\frac{\rho_v}{\rho_l}\right\}^{0.5}\left\{\frac{\mu_l}{\mu_v}\right\}^{0.1}. \tag{12}$$

Hence

$\Delta P_{fric} = \phi_l^2 \Delta P_{friclo}$,

ΔP_{fric} was resolved into the z and y directions,

$$\Delta P_{fricz} = \Delta P_{fric}\frac{GZ}{(GZ^2+GY^2)^{0.5}},$$

$$\Delta P_{fricy} = \Delta P_{fric}\frac{GY}{(GZ^2+GY^2)^{0.5}}.$$

Finally, Eqs. (4) and (3) were used to calculate the total pressure drop in the z and y directions.

3.2. Heat transfer coefficients

The flow boiling heat transfer coefficients were calculated using the superposition method, Eq. (13), as reviewed by Webb and Gupte (1992),

$$\alpha_{fb} = F\alpha_c + S\alpha_{npb}, \tag{13}$$

where α_c and α_{npb} are the single phase liquid only and nucleate pool boiling heat transfer coefficients respectively. Flow factor F represents the enhancement of α_c and suppression factor S the reduction of α_{npb} due to 2-phase flow effects. Although strictly only correctly applied to in-pipe flow, experimental data for crossflow have been shown by Jensen and Hsu (1988) to correlate well with the 2-phase friction multiplier,

$$F = \{\phi_l^2\}^{m/(2-n)}, \tag{14}$$

where m and n are the Reynolds number exponents for turbulent heat transfer and friction in single phase crossflow. Hero, the values $m = 0.8$ and $n = 0.2$ were used. The Bennett et al. (1980), correlation, Eq. (15), was used for S,

$$S = \frac{k_l}{F\alpha_c X_0}\left\{1 - \exp\left\{\frac{-F\alpha_c X_0}{k_l}\right\}\right\}, \tag{15}$$

where X_0 is the length of a region extending from the heated wall over which the average superheat is the driving force for nucleate boiling

$$X_0 = 0.041\left\{\frac{\sigma}{g(\rho_l - \rho_v)}\right\}^{0.5}, \tag{16}$$

α_c and α_{npb} are calculated using ESDU 73031 (ESDU, 1973) and the Mostinski (1963) correlation respectively. Since it is not known ab initio what proportion of the uniform heat flux q goes to nucleate and convective boiling, it is necessary to solve Eqs. (13)–(15) iteratively to determine wall superheat, δT.

4. Results and discussion

Using various boundary conditions, solutions were obtained for pentane and R113 boiling at 1 atm and at uniform heat fluxes of 20 and 50 kW/m^2. In all cases hydrostatic pressure was assumed to act at the bottom and sides of the bundle as justified above.

4.1. Pentane results

Solutions were obtained for the four boundary conditions of Table 1. Results for cases 1 and 4 are shown in Figs. 3 and 4.

Cases 1, 2 and 3 assume that flow enters and leaves the bundle vertically. Comparing cases 1 and 2 at $q = 50$ kW/m^2, in case 1 the vertical components of velocity just outside the bundle, $GZ(i+1, j)$ are assumed to be the same as those in the adjacent column inside the bundle whereas in case 2 they are negligible. Results for case 1 are shown in Fig. 3; the corresponding results for case 2 were identical to the scale of the plots. Flow within the bundle is insensitive to the flow just outside it. In case 3, $q = 20$ kW/m^2, reducing $GZ(i+1, j)$ to negligible values makes no significant difference to the data. The reason is that inertia pressure drops are small compared to friction and gravitational values.

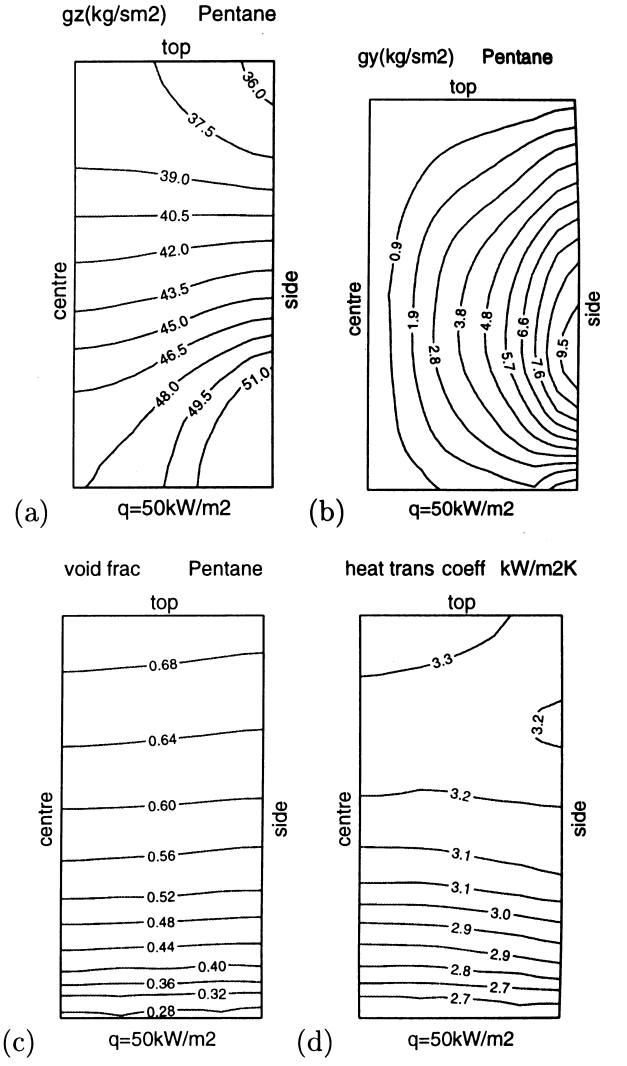

Fig. 3. Case 1 solution – Pentane, 1 atm, $q = 50$ kW/m^2 (average $\alpha_{fb} = 3.1$ kW/m^2 K).

Table 1
Solution boundary conditions, pentante

Solution no.	q (kW/m^2)	Boundary condition		
		Side	Top	Bottom
1	50	$GZ(N_C/2+1, j) = GZ(N_C/2, j)$	$GY = 0$	$GY = 0$
2	50	$GZ(N_C/2+1, j) = 1.0$	$GY = 0$	$GY = 0$
3	20	$GZ(N_C/2+1, j) = GZ(N_C/2, j)$	$GY = 0$	$GY = 0$
4[a]	20	$GZ(N_C/2+1, j) = 1.0$	Eq. (19)	Eq. (18)

[a] Based on $AR_t = AR_b = 1$ (Eqs. (19) and (18)).

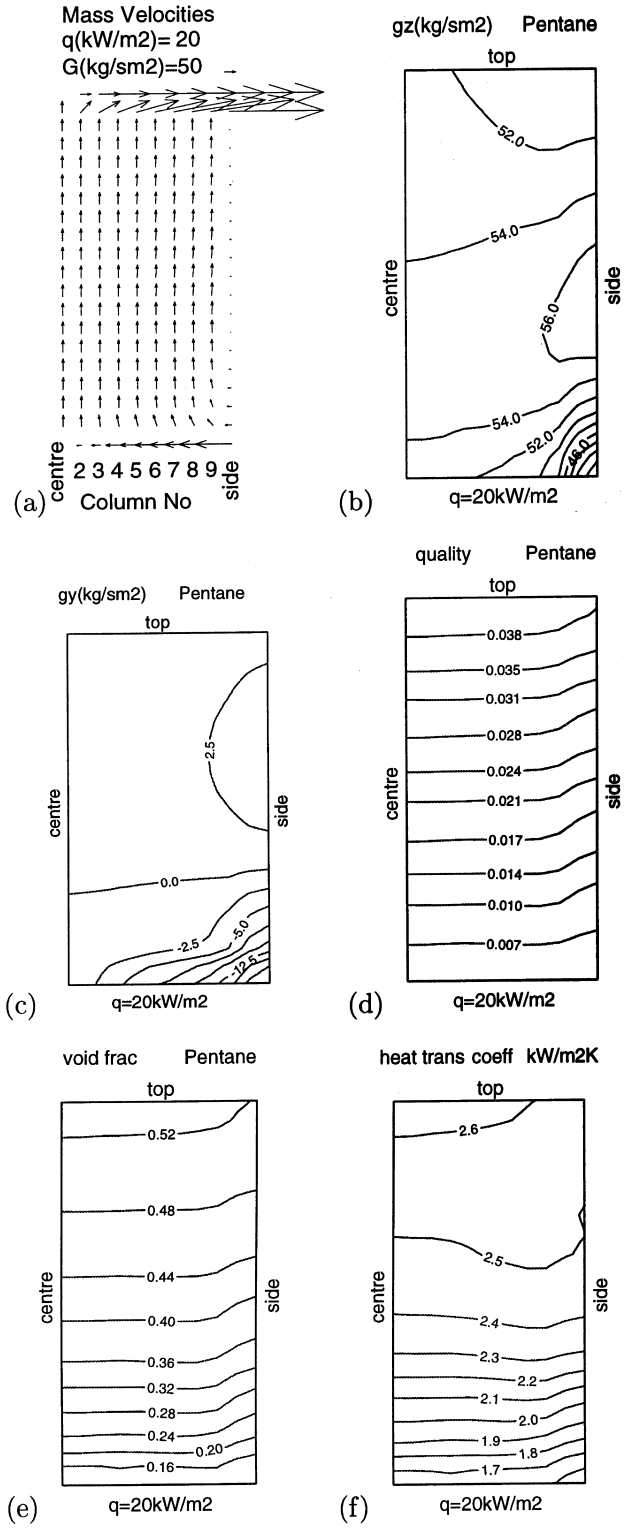

Fig. 4. Case 4 solution – Pentane, 1 atm, $q = 20$ kW/m^2 (average $\alpha_{fb} = 2.3$ kW/m^2 K).

At $q = 50$ kW/m^2 there are pronounced 2-D effects. Apart from row 1, column 9, everywhere there is a horizontal flow of fluid from the centre to the outside of the bundle, Fig. 3(b). This reaches a maximum of over GY = 11 kg/s m^2 at the outside of the middle rows, which is 22% of GZ entering the centre column, Fig. 3(a). As a result there is a progressive fall in vertical mass velocity between bundle top and bottom of 21% at the centre, 25% in column 5 and 30% in the outside column. Qualities and void fractions fall only slightly, laterally between the centre of the bundle and the side. This is because the vector mass velocity is not much reduced at the sides even though the vertical component is. The 1-D solution is a uniform mass velocity GZ of 39 kg/s m^2 and an exit quality and void fraction of 0.15 and 0.70, respectively, Table 2.

In the 2-D case, the egress of liquid at the sides reduces GZ all the way up the bundle and as a result the pressure drops are reduced. Hence, the average vertical mass velocity is 14% higher than the 1-D value. Quality at exit from the top row is on average 7% lower than the 1-D value. Void fractions at exit are about the same in the two cases, Table 2, due to the balancing effect of x and G, in the correlation, Eq. (6). The most significant comparison is that although the bundle average GZ is 14% higher in the 2-D case, the average heat transfer coefficient is the same as in the 1-D case, Table 2. In the 2-D case, higher G increases 2-phase friction factor ϕ_l^2 (Eqs. (11) and (12)), and hence flow factor F (Eq. (14)). The result is a small increase in the contribution of the convective boiling term α_c in Eq. (13) compared to the 1-D solution. There is a compensating reduction in wall superheat and hence in the nucleate boiling contribution. Hence, α_{fb} is largely unaffected by 2-D effects.

GY values are everywhere directed into the centre of the bundle below row 7 and outwards above at $q = 20$ kW/m^2. The results are very closely represented in Fig. 4 apart from the vector velocity values, Fig. 4(a), which shows the case 4 boundary condition on GB(i) and GY(i, 18) at the top and bottom. Ingress of fluid from the sides at the bottom is accompanied by outflow at the top, so that GZ peaks in the middle rows, Fig. 4(b). The 1-D solution gives a mass velocity of 51 kg/s m^2 and exit quality and void fraction of 0.044 and 0.52, respectively, Table 2. The average GZ value in the 2-D case is 53 kg/s m^2 and the average exit qualities, 0.044 and 0.54, respectively, Table 2. Effectively a 1-D solution in this case is satisfactory. Any 2-D effect is confined to flow in the outside columns. Again, bundle average heat transfer coefficients are the same for the two solutions, Table 2.

Using an asymptotic flow boiling correlation, Eq. (17),

$$\alpha_{fb} = \{\alpha_{npb}^2 + (F\alpha_c)^2\}^{0.5} \tag{17}$$

instead of the superposition one (Eq. (13)), reduced the 2-D average value of α_{fb} slightly to 2.9 at 50 kW/m^2 and 2.1 at 20 kW/m^2; the corresponding 1-D solution gave values of 2.8 and 2.1, respectively, again practically the same.

At $q = 50$ and 20 kW/m^2 the isolated tube values α_{npb} are 2.32 and 1.22 kW/m^2 K, respectively, so that as expected the bundle effect is large, especially at $q = 20$ kW/m^2. For the tube in column 5, row 9, for example, wall superheat is 8.73 K and the nucleate boiling contribution is only 12% of α_{fb}. At $q = 50$ kW/m^2, where ΔT is 17.0 K this rises to 45%. The superposition model predicts an even lower influence of nucleate boiling. This emphasises that the close agreement of 1-D and 2-D solutions is dependent mainly on similar vector velocities over the tubes and is by no means solely dependent on the nucleate boiling contribution.

4.1.1. Recirculation effects

Because of the recirculation of liquid there must be horizontal components of velocity below and above the bundle; the effect of these is examined in case 4, Table 1. Based on the boiler configuration of Shire et al. (1994), the average cross section of the flow between the bottom of the bundle and the shell was calculated to be 2.4 times the tube pitch. Using the

Table 2
Comparison of 1- and 2-D solution results, Pentane, 1 atm, $q = 50$ and 20 kW/m^2

Case	1-D solution				2-D solution			
	GZ_{av}	α_{fb}	x_{out}	ϵ_{out}	GZ_{av}	α_{fb}	x_{out}	ϵ_{out}
1	38.5	3.2	0.146	0.70	43.8	3.1	0.136	0.71
2	38.5	3.2	0.146	0.70	43.8	3.1	0.136	0.71
3	50.8	2.3	0.044	0.52	53.5	2.3	0.043	0.54
4	50.8	2.3	0.044	0.52	53.2	2.3	0.044	0.54

inlet mass velocities, $GZ(i,1)$, to columns i calculated in case 3, the horizontal components of velocities, $GB(i)$, below the bundle were determined by

$$GB(i) = -\left\{\sum_{i=1}^{i-1} GZ(i,1) + \frac{1}{2}GZ(i,1)\right\}/AR_b. \quad (18)$$

In case 4, AR_b was set to 1, to allow for non-uniform flow over the cross section below the bundle. Above the bundle, the liquid/vapour interface was assumed to be one tube pitch above the top row of tubes, $AR_t = 1$. The corresponding liquid flowrates, $GT_l(i)$ were calculated using Eq. (19) based on the liquid flowrates $\{1 - x(i,17)\}GZ(i,18)$ out of column i of the bundle and the qualities in the top row calculated in case 3.

$$GT_l(i) = \left\{\sum_{i=1}^{\frac{N_C}{2}} GZ(18,i) + \frac{1}{2}GZ(18,i)\right\}\{1 - x(i,17)\}/AR_t. \quad (19)$$

The resulting velocity vector and contour diagrams for case 4 are shown in Fig. 4. Corresponding qualities, void fraction and heat transfer coefficient contours are shown in these figures also.

In comparison with case 3, apart from the top row outlet and the bottom two rows, the velocity field in the bundle was found to be not greatly affected by the horizontal momentum of the recirculating liquid at top and bottom. The variation of GZ across the bundle and the pattern and values of GY are not much altered by the recirculation effect. At the side of the bundle, below row 3, there are some local effects of recirculation at the bottom but recirculation has an insignificant effect on flow inside the bundle at the top. In case 4, as in case 3, quality and void fraction are uniform across each row between the centre of the bundle and column 7, falling in the two outside columns, Fig. 4. Comparing cases 3 and 4, quality is only marginally lower at the top and bottom in case 4. Void fraction, which is very sensitive to quality at low qualities (Eq. (6)), is 25% lower in case 4 at the bottom of the bundle, rising to 2% lower in the middle and equal to the case 3 value at the top. There is no increase in two dimensionality of the flow in the bundle. The effect on flow boiling heat transfer coefficients is negligible, Table 2. Further, the recirculation rate is lower at $q = 50$ kW/m^2 so that the rate of horizontal momentum exchange above and below the boiler is lower and the recirculation effect no larger than at 20 kW/m^2.

4.1.2. Effect of recirculation on pressure boundary condition

So far it has been assumed that the bundle boundary pressures, $P_{side}(j)$ and $P_{bot}(i)$, are undisturbed pool hydrostatic pressures. To check this, the values of the recirculation flowrates based on case 3 calculated GZ and GY entering and leaving the bundle were superimposed on a simple model of the flowpath between shell and bundle. This consisted of a rough rectangular duct followed by a reducing elbow and an exhaust manifold feeding the columns of the bundle. 1-D flow was assumed with path lengths and widths equal to the average values for the configuration of Shire et al. (1994). The rough duct estimate was justified since the flowrate entering and leaving at the bundle sides is a small proportion of the average of the calculated values at top and bottom, 80 kg/s m^2. On this basis the friction pressure loss was claculated using Miller (1990) correlations to be 0.7 N/m^2 down the side, 33 N/m^2 in the elbow with a gradual pressure recovery to the end of the manifold due to the decrease in velocity. Thus the maximum increase of pressure over the hydrostatic value is 34 N/m^2 occurring below column 9 of the bundle. This is only 1.3% of the driving gravitational head of 2600 N/m^2 available and is further reduced nearer the centre columns. The deviation from hydrostatic pressure at the sides of the bundle is also negligible. On this basis it is concluded that the assumption of hydrostatic pool pressure levels around the bundle is reasonable at $q = 20$ kW/m^2. At higher heat fluxes the recirculating flowrate is lower. These observations are subject to the premise of this paper that disengagement of liquid from vapour is confined to the free surface so that there is little vapour presence in the space between bundle and shell.

4.2. R113 results

Solutions were obtained for R113 at 1 atm in the same configuration and for uniform heat fluxes of $q = 20$ and 50 kW/m^2, cases 5 and 6, Table 3.

Again the flow is almost 1-D at $q = 20$ kW/m^2. Contours of vertical and horizontal velocities, void fractions and heat transfer coefficients are shown in Fig. 5, $q = 50$ kW/m^2. Here there are significant 2-D effects. Due to lateral flow, GZ falls from bottom to top of the bundle by 20%, 24% and 27% in the centre, 5th and outside columns, respectively. The 1-D solution gives GZ = 100 kg/s m^2 and exit quality and void fraction of 0.140 and 0.69, respectively, compared to the 2-D averages of 112, 0.131 and 0.70. Average bundle heat transfer coefficients in the 1-D and 2-D cases are both 2.8 kW/m^2 K.

Table 3
Solution boundary conditions, R113

Solution no.	q (kW/m^2)	Boundary condition		
		Side	Top	Bottom
5	50	$GZ(N_C/2+1, j) = GZ(N_C/2, j)$	$GY = 0$	$GY = 0$
6	20	$GZ(N_C/2+1, j) = 1.0$	$GY = 0$	$GY = 0$

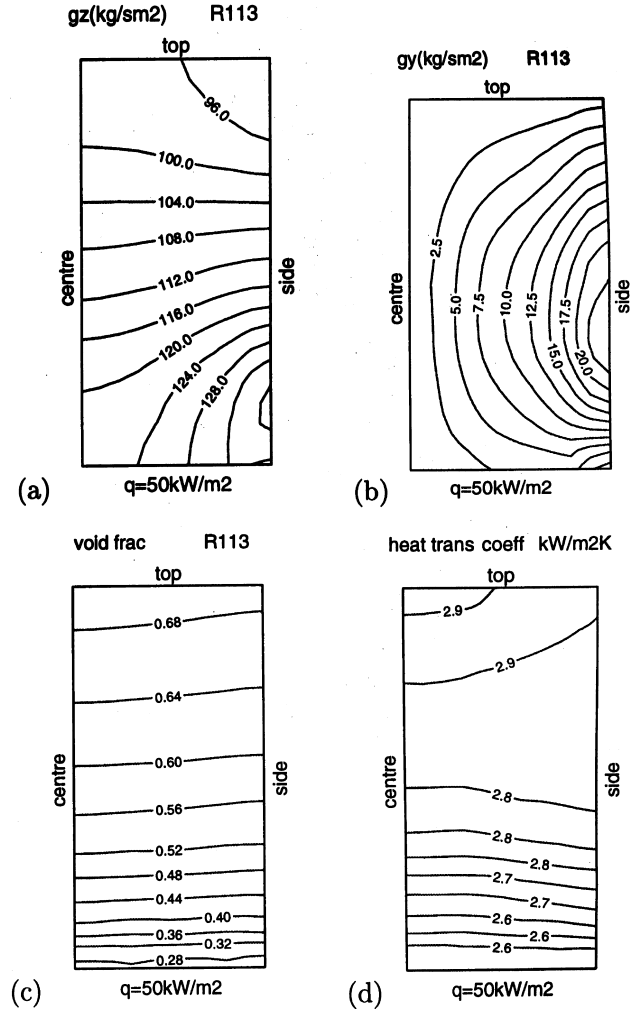

Fig. 5. Case 5 solution – R113, 1 atm, $q = 50$ kW/m^2 (average $\alpha_{fb} = 2.8$ kW/m^2 K).

Based on minimum flow area, $G_{max} = \{G/(1 - D/s_h)\}$, entering the bundle at the bottom in the 2-D solution averages 510 kg/s m^2 at 50 kW/m^2 and 500 kg/s m^2 at 20 kW/m^2. Table 4 shows this result compared to directly measured values and the predictions of Brisbane et al. (1980) which, in a sense, were the best fit of the 1-D model to the data of Leong and Cornwell (1979) and Cornwell et al. (1980). This author suspects these data values are too high because there was a high unknown heat loss from the back of the boiler in the experiments. This meant that the average q was considerably lower than the nominal values. Thus the average values of G estimated from the data for both heat fluxes are too high. In confirmation, the very high values of α_{fb} reported by Leong and Cornwell (1979) near the top of the bundle were caused by high heat loss, resulting in lower calculated tube wall superheats. More recent data measured in this author's laboratory and elsewhere gives much less variation in α_{fb} from bottom to top of the bundle. The Shire et al. (1994) LDA data quoted is the value measured entering the centre columns of the bundle. Although mass velocity continuity checks of the data in this region agreed within 6% at 20 kW/m^2 and 14% at 50 kW/m^2, the accuracy is probably lower than this because vertical and horizontal components of velocity had to be measured in separate experiments in each of which it took several minutes to make the necessary traverses. Clearly, predictions of the present model are lower than measured values. However, experimental errors are high and difficult to assess. Bearing in mind that the purpose of the present study is to determine 2-D effects, these differences are not judged to be significant. The level of mass velocities predicted is a function of the particular 2-phase flow correlations used.

The discussion would not be complete without comparison with the predictions of the more elaborate models of Carlucci et al. (1984), King and Jensen (1995) and Rahman et al. (1996). None of these authors attempted to model the disengagement process above the bundle in which surface tension forces are dominant. Vapour disengages from the froth by coalescence of bubbles, preceded by surface tension induced flow of liquid film between them until it reaches a critical thickness at which coalescence can occur. Flow in the axial direction towards the weir and the effect of geometry of the shell above the bundle must be factors in a successful analysis also. Despite this, Carlucci et al. (1984), based on Leong and Cornwell's configuration at $q = 20$ kW/m^2, predicted a continuous liquid phase at the side of the bundle. This was even though their void fraction of fluid leaving the bundle was too high due to the assumption of homogeneous flow. Consequently, they predicted a recirculation rate greater than the measurements of Cornwell et al. (1980) and Shire et al. (1994). At uniform wall superheat of 10 K, average $q = 50$ kW/m^2, Edwards and Jensen (1991), Fig. 5, predicted similarly that there was a continuous liquid phase path from top to bottom at the sides of the shell. The recirculation mass velocity is difficult to assess from their paper since the length of the shell analysed was not given. However, as determined here, Table 4, there was little difference between the values at 20 and 50 kW/m^2. Rahman et al. (1996) used their interfacial friction correlation in a similar analysis for R113 at $q = 20$ kW/m^2. They predicted the frothy high voidage region observed by Leong and Cornwell (1979). Since the confined nature of the experimental slice was not conducive to disengagement, the lack of a disengagement model in the analysis was not important. However, as discussed above, the situation is different in full scale kettle reboilers, where the build up of froth is likely to be far less severe. In these circumstances and until a suitable disengagement model can be devised, it seems adequate to base prediction of flow and heat transfer in kettle reboilers operating on moderate heat fluxes on models of the type described here.

5. Conclusions

Assuming that liquid/vapour disengagement is not severe enough to influence the hydrostatic driving force for recirculation, a simple 2-D adaption of the standard 1-D prediction

Table 4
Predicted G_{max} v. measured data, R113, 1 atm

Source	Leong and Cornwell (1979)	Cornwell et al. (1980)	Cornwell et al. (1980)	Brisbane et al. (1980)		Shire et al. (1994)		This work	
q	20	20	50	20	50	20	50	20	50
G_{max}	590	680	640	580	400	570	660	510	500

model has been developed for 2-phase flow in a kettle reboiler. Flow over the bundle tubes is shown to be relatively unaffected by conditions in the shell outside, for a typical geometry. Recourse to CFD software is therefore considered unnecessary to the accuracy of 2-phase flow correlations which are at present required in any solution. Uniform heat flux solutions for pentane and R113, each 1 atm, reveal that there are pronounced 2-D effects on mass velocity within the bundle at $q = 50$ kW/m^2 but these are negligible at 20 kW/m^2. Using typical superposition and asymptotic flow boiling models, the 2-D model predicted the same bundle average heat transfer coefficients as the 1-D solution at both heat fluxes. However, the effect of reduction in vertical mass velocity at the top of the bundle predicted by the 2-D solution is important in predicting design maximum heat flux.

Acknowledgements

The author thanks Dr. Alastair Martin and Mr. Keith Miller for their help in implementing the Newton–Broyden solution and preparing the manuscript and EPSRC and HTFS for supporting the work.

References

Bennett, D.L., Davis, M.W., Hertzler, B.L., 1980. The suppression of saturated nucleate boiling by forced convective flow. AIChE Symp. Ser. 26 (199), 91–103.

Brisbane, T.W.C., Grant, I.D.R., Whalley, P.B., 1980. A prediction method for kettle reboiler performance. ASME Paper No. 80-HT-42.

Carlucci, L.N., Sutherland, D., 1981. The effects of various empirical correlations on the predictions of a steam generator thermal-hydraulics code. ASME Paper No. 181-WA/NE-5.

Carlucci, L.N., Galpin, P.F., Brown, J.D., 1984. Numerical predictions of shellside heat exchanger flows. In: A Reappraisal of Shellside Flow in Heat Exchangers. ASME Publ. HTD 36, 19–26.

Cornwell, K., Duffin, N.W., Schuller, R.B., 1980. An experimental study of the effects of fluid flow on boiling within a kettle reboiler tube bundle. ASME Paper No. 80-HT-45.

Dowlati, R., Kawaji, M., Chan, A.M.C., 1990. Pitch-to-diameter effect on two-phase flow across an in-line tube bundle. AIChE J. 36, 765–772.

Dowlati, R., Chan, A.M.C., Kawaji, M., 1992a. Hydrodynamics of two-phase flow across horizontal in-line and staggered rod bundles. TASME J. Fluids Eng. 114, 450–456.

Dowlati, R., Kawaji, M., Chisholm, M., Chan, A.M.C., 1992b. Void fraction prediction in two-phase flow across a tube bundle. AIChE J. 38 (4), 619–622.

Edwards, D.P., Jensen, M.K., 1991. A two dimensional model of two-phase heat transfer and fluid flow in a kettle reboiler. In: Phase Change Heat Transfer. ASME Publ. HTD 159, 9–16.

ESDU 1973. Convective heat transfer during crossflow of fluids over plain tube banks. Item no. 73031 Eng. Sci. Data Unit, London.

ESDU 1979. Crossflow pressure loss over banks of plain tubes in square and triangular arrays including effects of flow direction. Item no. 79034, Engineering Sciences Data Unit, London.

Hadi, H.A., Burnside, B.M., 1992. Predictions of in-tube circulation models compared to performance of an experimental kettle reboiler model. Heat Transfer, Proc. Third UK and First European Thermal Sciences Conf. 1, pp. 197–207.

Ishihara, K., Palen, J.W., Taborek, J., 1980. Critical review of correlations for predicting two-phase pressure drop across tube banks. Heat Transfer Eng. 1, 23–32.

Jensen, M.K., Hsu, J-T., 1988. A parametric study of boiling heat transfer in a horizontal tube bundle. TASME J. Heat Trans. 110, 976–981.

King, M.P., Jensen, M.K., 1995. Local heat transfer and flow pattern distributions in a kettle reboiler. Two Phase Flow Modelling and Experimentation 2, 1289–1296.

Lahey, R.T. Jr., Drew, D.A., 1988. The three-dimensional time and volume averaged conservation equations of two-phase flow. In: Lewins, J., Becker, M. (Eds.), Advances in Nuclear Science and Technology 20. Plenum Press, London.

Leong, L.S., Cornwell, K., 1979. Heat transfer coefficients in a reboiler tube bundle. Chem. Engnr. 343, 219–221.

Miller, D.S., 1990. Internal Flow Systems. BHRA, Bedford.

Mostinski, I.L., 1963. Application of the rule of corresponding states for the calculation of heat transfer and critical heat flux. Teploenergetika 4, 66–71 [English Abstract, Br. Chem. Eng. 8, 580].

Palen, J.W., Yang, C.C., 1981. Circulation boiling model for analysis of kettle and internal reboiler performance. In: Heat Exchangers for 2-phase Applications. ASME Publ. HTD 27, 55–61.

Rahman, F.H., Gebbie, J.G., Jensen, M.K., 1996. An interfacial friction correlation for shell-side vertical two-phase cross-flow past horizontal in-line and staggered tube bundles. Int. J. Multiphase Flow 22 (4), 753–766.

Schrage, D.S., Hsu, J.-T., Jensen, M.K., 1988. Two-phase pressure drop in vertical crossflow across a horizontal tube bundle. AIChE J. 34 (1), 107–115.

Shire, N.F., 1995. Heat transfer and hydrodynamics of flow over tube bundles. Ph.D. Thesis, Heriot-Watt University.

Shire, N.F., Burnside, B.M., Didsbury, R., 1994. Circulation velocity measurements in a model multitude reboiler using laser doppler anemometry. Heat Transfer 1994, Procs. 10th Int. Heat Trans. Conf. 7, pp. 539–544.

Singhal, A.K., Spalding, D.B., 1979. Mathematical modelling of multi-phase flow and heat transfer in steam generators. Multi-phase Transport-Fundamentals, Reactor Safety, Applications, Procs. Multi-phase Flow and Heat Transfer Symp. 1, pp. 373–406.

Webb, R.L., Gupte, N.S., 1992. A critical review of correlations for convective vaporisation in tubes and tube banks. Heat Transfer Eng. 13, 58–81.